



Wear Resistance of Boron-Modified Supermartensitic Stainless Steel Coatings Produced by High-Velocity Oxygen Fuel Process

G. Y. Koga¹ · G. Zepon¹ · L. S. Santos¹ · C. Bolfarini¹ · C. S. Kiminami¹ · W. J. Botta¹

Submitted: 5 July 2019/in revised form: 12 November 2019/Published online: 26 November 2019
© ASM International 2019

Abstract The wear resistance of boron-modified supermartensitic stainless steel coatings produced by high-velocity oxygen fuel (HVOF) was investigated through pin-on-disk measurements. It was shown that addition of boron leads to the formation of an interconnected and rigid boride network delimiting the grain boundaries of the martensitic matrix. A very refined structure was formed as result of the high cooling rates imposed to the molten alloy during the HVOF process. The specific wear rates of the HVOF coatings were about tenfold lower than the boron-free supermartensitic stainless steel, lying in the order of 10^{-5} mm³/N m. The refined boride skeleton along the HVOF coating was found to be effective to reduce the materials' removal from the exposed softer martensitic matrix. While the supermartensitic stainless steel master alloy and the mild steel substrate displayed severe adhesive wear, the HVOF coatings exhibited mild delamination wear at low sliding velocities (10 and 20 cm/s) and abrasive wear at the highest tested velocity (40 cm/s). The studied boron-modified supermartensitic HVOF coatings are an interesting approach to protect the surface of inexpensive steel substrates against wear.

Keywords boride · HVOF · stainless steel · wear-resistant coatings

Introduction

High corrosion and wear resistances are basic requirements of materials operating in aggressive environments such as those found in the petrochemical industry (Ref 1, 2). Among the commercially available alloys, stainless steels are well-established candidates for applications where good mechanical properties and high corrosion resistance are demanded (Ref 3, 4). Although largely used, conventional stainless steel grades are not generally regarded as wear-resistant materials, even though some of those alloys can be cold-worked (ferritic and austenitic) or heat-treated (martensitic) to improve their hardness (Ref 5).

An interesting approach proved to effectively increase the wear resistance of stainless steels is the use of minor additions of boron to form hard phases (Ref 6). Having low solubility in Fe-based alloys, the addition of boron to the stainless steel grades leads to the formation of M₂B-type phases, where *M* is composed of the transition metals usually present in stainless steels such as Fe, Cr, Nb and Mo. Stainless steels of different classes [ferritic (Ref 7, 8), supermartensitic (Ref 9, 10) and superduplex (Ref 11–13)] can be modified by boron addition to induce boride-reinforced microstructures resistant to wear. Indeed, boriding is one of the most effective methods for increasing the wear resistance of steel parts due to the formation of hard borides such as Fe₂B (1600 HV) and FeB (1800 HV) (Ref 14). To date, the most explored processing route to produce boron-modified stainless steel has been spray forming because of the unique characteristics of the resulting microstructure (Ref 15, 16). This includes the formation of a non-dendritic refined microstructure with low levels of segregation and the possibility to homogeneously disperse second phases such as borides.

✉ G. Y. Koga
gykoga@ufscar.br

¹ Department of Materials Science and Engineering, Federal University of São Carlos, Rod. Washington Luis, km 235, São Carlos, SP CEP 13565-905, Brazil

Besides spray forming, thermal spraying techniques are an interesting route to produce wear-resistant alloy coatings (Ref 17, 18). High-velocity oxygen fuel (HVOF) is efficient, among thermal spraying methods, to induce refined and dense protective coatings due to the high velocity of the particles and the elevated cooling rate upon deposition (Ref 19). Another advantage of the HVOF process is that structural components made with inexpensive steels and with complex geometry can be coated with protective and relatively thin advanced alloys (Ref 20). Since most failures of structural materials initiate from the surface, the use of a HVOF coating of a more noble alloy deposited onto an inexpensive one is an interesting low-cost engineering solution to extend the service life of large structural components operating in harsh conditions (Ref 21–24). Protective Fe-based HVOF coatings with boron deposited onto low-carbon steels have been intensively studied (Ref 25–30). However, the production of boron-modified supermartensitic stainless steel HVOF coatings resistant to wear has not been largely reported.

In this work, the wear resistance of a boron-modified supermartensitic stainless steel HVOF coating was evaluated through pin-on-disk tests. The AISI 1010 carbon steel used as substrate and the supermartensitic stainless steel considered as master alloy were also tested as terms of comparison. The results were discussed based on the composition and processing route to justify why the boron-modified supermartensitic stainless steel HVOF coatings are an interesting surface engineering solution to be used as wear-resistant material.

Experimental Procedure

HVOF Process

A commercial supermartensitic stainless steel was modified with boron addition and processed by spray forming using N₂ as atomization gas, pouring temperature 1564 °C, nozzle diameter 4 mm, atomization pressure 0.6 MPa, melt flow rate 0.11 kg s⁻¹ and gas-to-metal ratio about 3.54. Iron-boron, iron-molybdenum and commercial pure chromium and nickel were used to adjust the composition. The resulting overspray powder produced from this process was used as feedstock precursors, after proper sieving to select particles between 20 and 53 μm, in an HVOF process to coat mild steel plates (100 × 100 × 5 mm) previously sandblasted and methanol-degreased. The term “overspray” means the non-deposited particles result from spray forming to produce bulk parts. Table 1 summarizes the ensemble of the parameters considered in the HVOF process. Figure 1 presents the microstructure and the

Table 1 Spraying parameters employed in the HVOF process

HVOF process	
Gun barrel, cm	10.16
Standoff distance, mm	355
Torch velocity, mm/s	555
Oxygen, Pa	8.9×10^5
Kerosene, Pa	7.8×10^5
Combustion pressure, Pa	6.7×10^5
Oxygen flow, m ³ /min	51
Kerosene consumption, L/min	3.2×10^{-1}
Spray rate, g/min	152
Carrier gas	Argon
Coating thickness, μm	982 ± 38

A JP-5000 HP/HVOF system, TAFE torch model 5220 from Praxair Surface Technology, was used to produce the thermally sprayed coatings onto the mild substrate initially at room temperature

composition of the mild steel substrate and of the supermartensitic stainless steel master alloy.

Chemical composition of the feedstock powder was determined by different techniques. Carbon content was measured by high-temperature combustion followed by infrared detection. The content of the remaining elements was determined by inductive-coupled plasma atomic emission spectroscopy (ICP-AES), except for boron that was assessed by atomic absorption spectroscopy (AAS). Table 2 presents the chemical composition of the feedstock powder. Oxidation and boron loss are the main causes of compositional deviations during HVOF processing of boron-containing stainless steels; therefore, the oxygen and boron contents of the resulting coatings were quantified by inert gas fusion method and AAS, respectively.

X-ray diffraction was performed in a Bruker D8 ADVANCE diffractometer using Cu-Kα radiation to allow phase identification. The microstructure of the HVOF coatings was evaluated by a field emission gun (FEG) scanning electron microscope (SEM) Philips XL30 equipped with a Bruker XFlash 6160 EDS detector. The porosity level of the coatings was estimated from six cross-sectional micrographs by optical microscopy (magnification of 200×) using the ImageJ image processing program.

Wear Measurements

Hardness measurements were performed in different regions of 1 μm-Al₂O₃ polished samples using a Vickers diamond indenter equipped onto a Shimadzu HVM-G20ST tester, with 300 g load and 15 s dwell time. At least six measurements for each sample type were allowed to

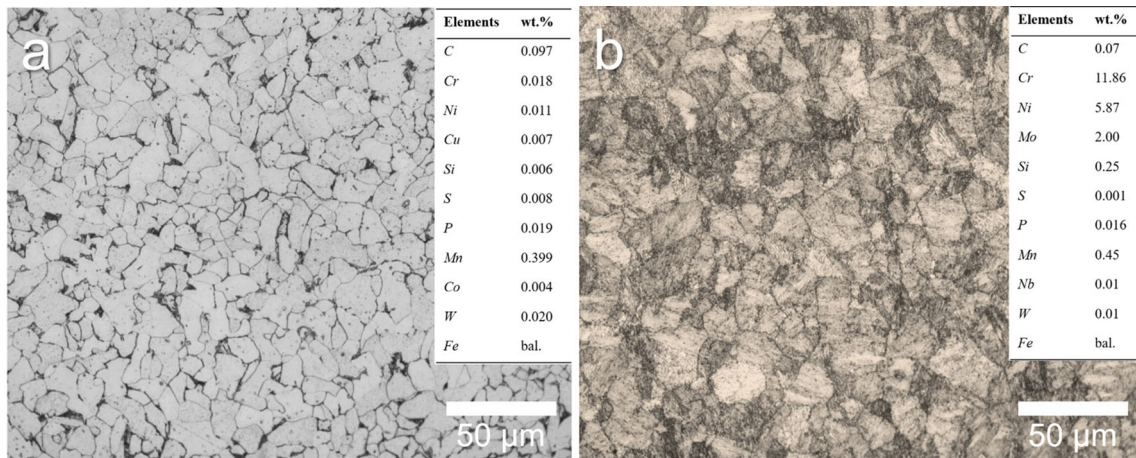


Fig. 1 Optical micrographs of (a) the AISI 1010 steel used as substrate for the HVOF coating deposition, and (b) of the commercial supermartensitic stainless steel used as master alloy. Both materials were used in wear testing as references. Etching: AISI 1010 (Nital 5%) and supermartensitic stainless steel (Vilella). Chemical

compositions determined by spark optical emission spectrometry, excepted for the carbon and sulfur contents that were estimated by high-frequency induction furnace and infrared detection system. Density measured by pycnometry: AISI 1010 ($\rho = 7.722 \pm 0.007 \text{ g/cm}^3$) and supermartensitic stainless steel ($\rho = 7.842 \pm 0.004 \text{ g/cm}^3$)

Table 2 Measured composition, in wt.%, of the resulting feedstock powders (FP)

Samples	%C	%Cr	%Ni	%Mo	%B	%Ti	%Mn	%S	%Fe	ρ^* , g/cm ³
FP	0.039	13.56	5.42	1.82	0.71	0.040	0.52	0.002	Bal.	7.82

*Presented as the mean value from five measurements in a pycnometer Micromeritics Accupyc 1330

present the results as mean values and their standard deviations.

Pin-on-disk measurements were carried out on 1- μm Al₂O₃ polished disks ($\varnothing 50 \times 8 \text{ mm}$, Fig. 2) in a Plint TE 67 microprocessor controlled machine at room temperature ($T = 20 \pm 2 \text{ }^\circ\text{C}$) and under dry sliding conditions ($60 \pm 5\%$ relative humidity). After polishing, the average roughness (R_a) of the HVOF and 1010 steel disks were $0.42 \pm 0.05 \text{ }\mu\text{m}$ and $0.11 \pm 0.02 \text{ }\mu\text{m}$, respectively.

Alumina balls (purity Al₂O₃ > 99%) of 5.4 mm in diameter with R_a of $0.12 \pm 0.03 \text{ }\mu\text{m}$ and $1560 \pm 70 \text{ HV}_{0.3}$ were used as counter-face pins. A total distance of 1000 m and a load of 9.8 N were considered in three different linear sliding velocities: 10, 20 and 40 cm/s.

Worn volume was determined considering the density values obtained by gas pycnometry (AccuPyc II 1340 Pycnometer) and the measured mass loss. The specific wear rate, K , after each test was calculated by the equation $K = V/(F \times L)$, where V is the volume loss (mm³), F is the normal load (N) and L is the total sliding distance (m). Replicate measurements for each sample and at each wear condition were performed to ensure repeatability. X-ray diffraction patterns of the debris and SEM images of the worn surfaces, both acquired using the equipment mentioned before, were employed to identify the wear mechanisms. Confocal microscopy was used as complement to analyze the width and depth of the worn track, using a LEXT 3D Measuring LASER microscopy OLS4100 Olympus.

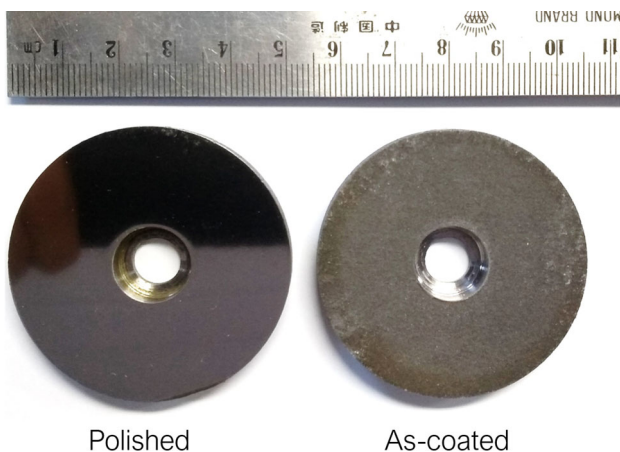


Fig. 2 HVOF disk samples used in the pin-on-disk tests. Ruler in cm

Results

Microstructure

Figure 3 shows the XRD patterns of the feedstock powder (FP) and of the resulting HVOF coatings. Well-pronounced peaks related to martensite are seen for the boron-modified supermartensitic alloy regardless of the processing route. Besides keeping the martensitic patterns as for the supermartensitic stainless steel (SM SS) master alloy, the boron-modified samples displayed peaks associated with borides of metallic alloy's components (e.g., Fe, Cr, Ni, Mo) and related to retained austenite.

The microstructure of the boron-modified supermartensitic stainless steel feedstock powders and of the HVOF coating is detailed in Fig. 4. The near-spherical and relatively smooth nature of the particles selected as feedstock powder is highlighted in Fig. 4(a) as well as the proper size range between 20 and 53 μm after sieving. A cross-sectional view of a feedstock particle in Fig. 4(b) reveals a refined microstructure composed of a martensitic matrix surrounded by an interconnected boride network delimitating the grain boundaries. Some boron loss occurred upon the coating deposition, from 0.71 wt.% of the feedstock powder to 0.51 wt.% for the resulting coating. Thick HVOF coatings, $\sim 1000 \mu\text{m}$, were produced as seen in Fig. 4(c) and (d), where features characteristic of the thermal spraying route is observed. The inset in Fig. 4(d) allows to better observe the lamellar structure composed of regions that were built from fully molten (featureless area, see region 1), partially molten (deformed particles, follow arrow 2) and un-molten spherical

particles, follow arrow 3; porosity is also visible since it is an inherent drawback related to any thermal spraying method such as the HVOF (see arrow 4). The estimated porosity of the coatings, from image analyses on six different cross-sectional optical micrographs, was $5 \pm 1\%$.

An intrinsic variation in the size and thermal history exists for each individual particle upon spraying deposition to build up the HVOF coating. Depending on these characteristics, the particles impact the substrate in the molten, partially molten or un-molten states. Figure 5 shows the microstructure of the three main constituents that form the HVOF coatings. A similar microstructural characteristic is seen regardless of the state that the particles reached the substrate, i.e., the boride network delimiting the grain boundaries of the martensitic phase. For the un-molten particle, Fig. 5(a) and (b), the equiaxial morphology displayed by the feedstock powder (Fig. 4b) persists, except at the outmost region of the particle, where deformation of the microstructure occurred due to the impact against the forming coating. The region formed from the molten particle exhibited a more distorted microstructure, Fig. 5(e) and (f), while that related to the partially molten particle, Fig. 5(c) and (d), is in between the features from the un-molten and molten particles.

Figure 6 shows the characteristics of an intersplat zone. The thickness of this region is not uniform, Fig. 6(a), as well as the distribution of the main elements of the alloy, Fig. 6(b). Compared to the inner region, the intersplat is rich in oxygen because of oxidation upon deposition at high temperatures. Besides oxygen, the intersplat contains Fe, Cr, Mo and Ni, stated here in decreasing order.

Wear

The measured hardness values of the boron-modified supermartensitic stainless steel samples produced by HVOF, AISI 1010 steel substrate and the supermartensitic stainless steel used as master alloy are compiled in Fig. 7. Among the tested alloys, the mild steel substrate displayed the lowest hardness values, around 170 $\text{HV}_{0.3}$, followed by the supermartensitic stainless steel master alloy with mean hardness value around 270 $\text{HV}_{0.3}$. The highest values were displayed by the HVOF coatings ($\sim 530 \text{HV}_{0.3}$).

Figure 8a shows the specific wear rates, K , from pin-on-disk tests at different linear sliding velocities (10, 20 and 40 cm/s), and the coefficient of friction, COF , along the 1000 m of sliding distance, Fig. 8(b) to (d). Among the tested samples, the HVOF coatings displayed the lowest K values, ranging between $4 \times 10^{-5} \text{mm}^3/\text{N m}$ and $8 \times 10^{-5} \text{mm}^3/\text{N m}$. The latter value is associated to the highest sliding velocity. The K values of AISI 1010 substrate and the supermartensitic stainless steel master alloy (SM SS) increased with the linear sliding velocity, and they

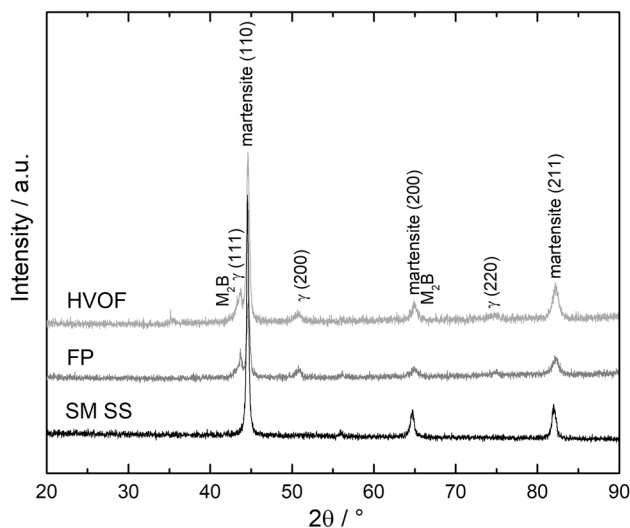
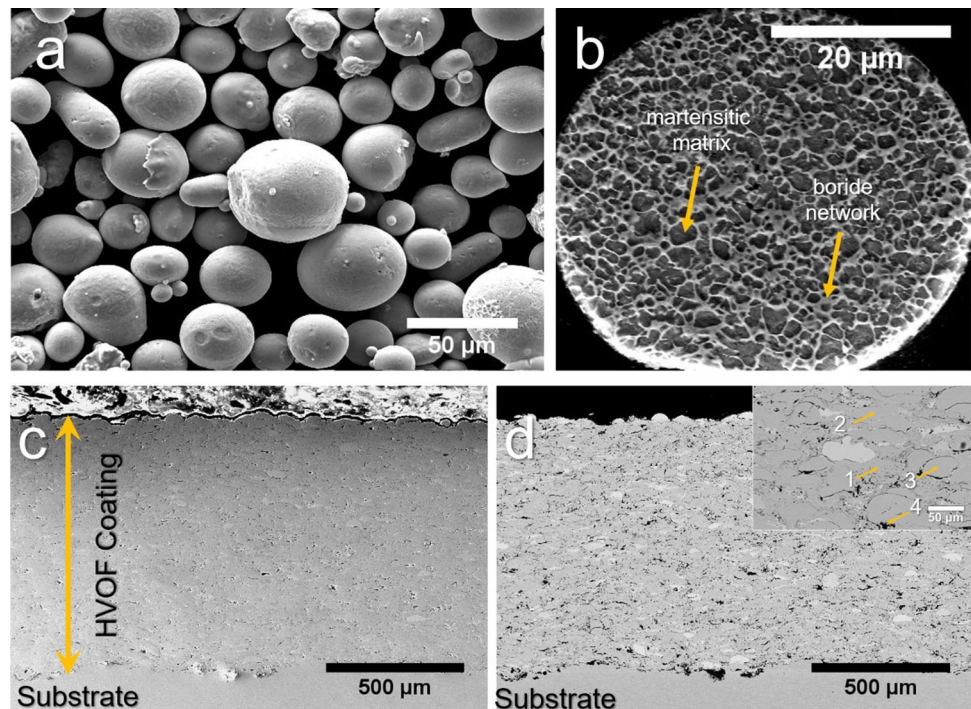


Fig. 3 X-ray diffraction patterns of the boron-modified supermartensitic stainless steel (SM SS) in form of feedstock powder (FP) and HVOF coatings. M_2B stands for borides composed mainly by Fe and Cr, with small amounts of Ni and Mo

Fig. 4 (a) Secondary electron SEM micrograph of selected boron-modified supermartensitic stainless steel particles used as feedstock powder, and (b) a cross-sectional view of a particle to highlight the refined boride network (etched with aqua regia reagent, 1 HNO₃:3 HCl, in volume). Cross-sectional secondary electron (c) and backscattered electron (d) SEM micrographs of the resulting HVOF coating



were about tenfold superior than those of the protective HVOF coating. The *COF* evolution along the testing distance was similar for all samples with martensitic stainless steel matrix regardless of the sliding velocity. The average *COF* value was close to the unity, Fig. 8(b) and (c), except for the HVOF coating tested at 40 cm/s, Fig. 8(d), that displayed a slightly lower *COF* value with some fluctuations along the testing distance. AISI 1010 steel exhibited comparable steady-state values of *COF* around 0.5 regardless of the sliding velocity. These *COF* values are in the range of what is expected for steel materials sliding against a ceramic counterpart in air and in the absence of lubricant (Ref 31).

Analyses of the wear track of the AISI 1010 and HVOF coating tested at the lowest (10 cm/s) and at the highest (40 cm/s) sliding velocities are shown in Fig. 9. For both materials, a substantial increment in the depth and width of the wear track is seen with increasing sliding velocity. The HVOF coating displayed a narrower and shallower worn surface, especially for the highest sliding velocity, with the width of 1384 μm and depth of 6.8 μm against 2143 μm width and 74.9 μm depth for the AISI 1010 steel substrate.

Discussion

The cooling rates experienced upon the deposition of particles to form coatings through HVOF are in the order of 10^4 to 10^6 K/s (Ref 32). The microstructure of the HVOF coating is composed of martensitic matrix within borides

delimiting the grain boundaries, Fig. 5. The high cooling rate imposed during deposition resulted in a refined microstructure for the HVOF coating. The presence of hard borides combined with the refined microstructure allowed the HVOF coatings to display hardness values considerably superior, almost twofold, compared to those related to the supermartensitic stainless steel master alloy and the AISI 1010 steel substrate. The low hardness value of AISI 1010 steel is attributed to the low-carbon content and, therefore, the reduced pearlite fraction as seen in Fig. 1(a). Even with a martensitic microstructure, Fig. 1(b), the master alloy also possesses a reduced carbon content to reduce the risk of sensitization, so the structure of the martensite is not considerably deformed to effectively reduce the dislocations' movement.

A pronounced improvement in the wear resistance is achieved through boron modification of the supermartensitic stainless steel used as protective HVOF coating. This is attributed to the refined, rigid and interconnected boride skeleton along the coatings' grain boundary, acting as an effective barrier against material removal. The refinement of the boride network within the matrix is a key aspect to be considered to design wear-resistant boron-modified alloys. This aspect has been raised by Zepon et al. (Ref 10) where different boron-modified supermartensitic stainless steels produced by spray forming were tested against dry sand in a wheel abrasive wear test and in plate-on-cylinder configuration. It was found that in the case of the dry sand/rubber wheel abrasive wear test little difference between the wear resistance of the supermartensitic master alloy and

Fig. 5 Secondary electron SEM micrographs taken from a cross-sectional region of the HVOF coating revealing the microstructure of different constituents originated from: (a, b) un-molten particle, (c, d) partially molten particle and (e, f) fully molten particle. An etching of HCl and HNO₃, in a proportion 3:1 in vol., was used to better reveal the boride network

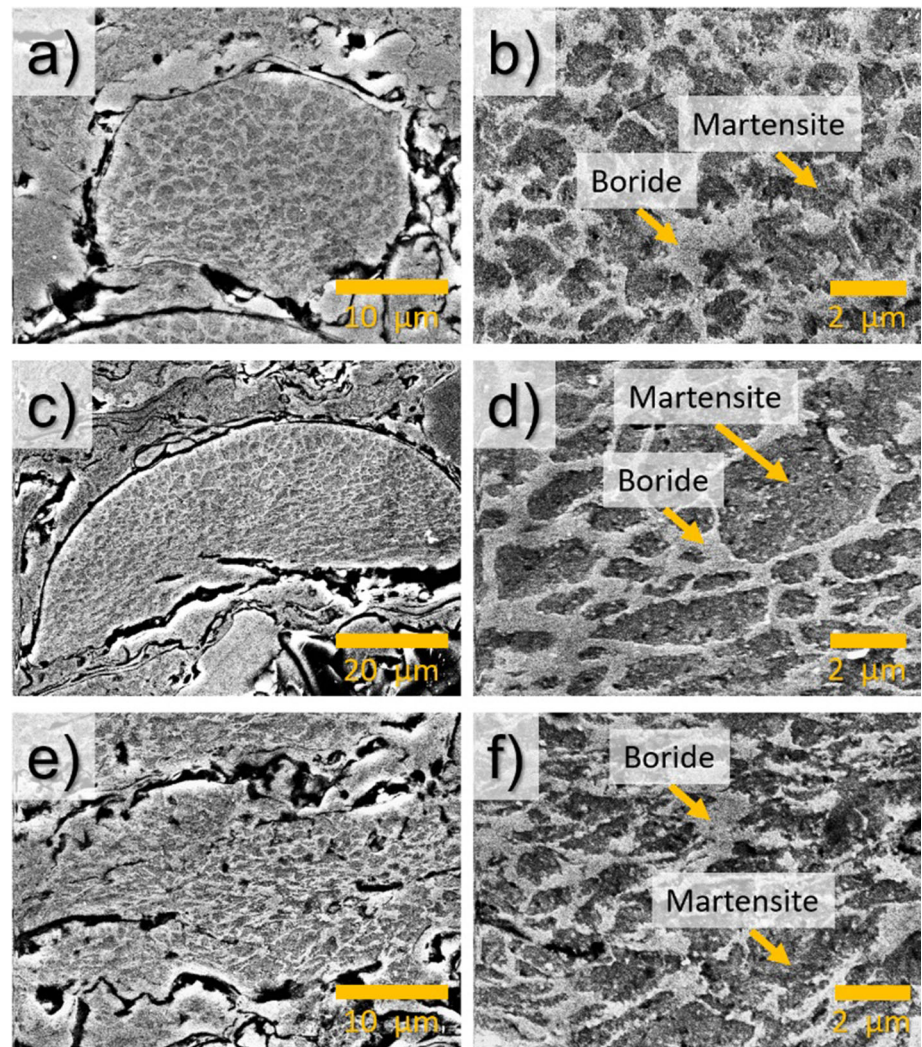
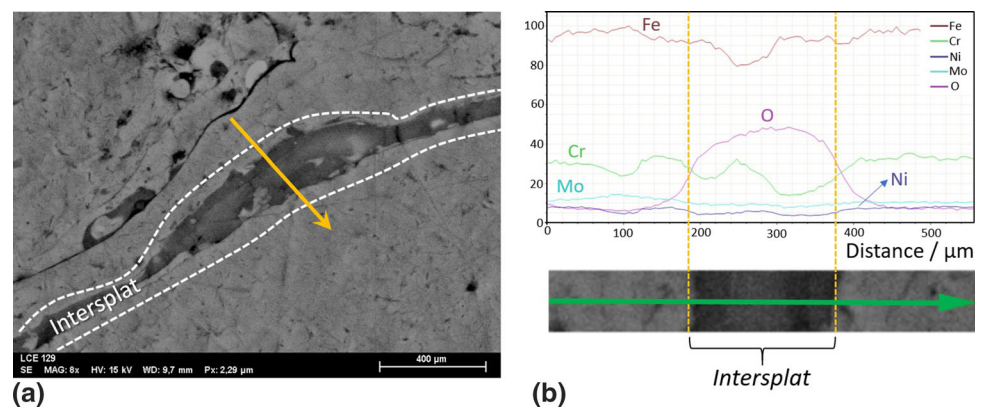


Fig. 6 (a) SEM micrograph highlighting the intersplat zone in the HVOF coating, and (b) the elemental line scan through the intersplat zone [along the arrow in (a)], considering the major components of the alloy (Fe, Cr, Ni, Mo) and oxygen



the boron-modified one could be seen, while in the plate-on-cylinder wear test the behavior of the latter was much superior to the first. Even if coarser than in the HVOF coating, the boride network in spray-formed deposits is efficient to restrain the material removal in applications involving large surface contact between the moving parts.

The worn surfaces in Fig. 10 and the XRD patterns of the debris in Fig. 11 bring elements to discuss about the wear mechanisms. Adhesive wear is preponderant in the supermartensitic stainless steel as revealed by the tracks of large plastic deformation in the contact region under compression and shearing (see Fig. 10a-c). XRD patterns

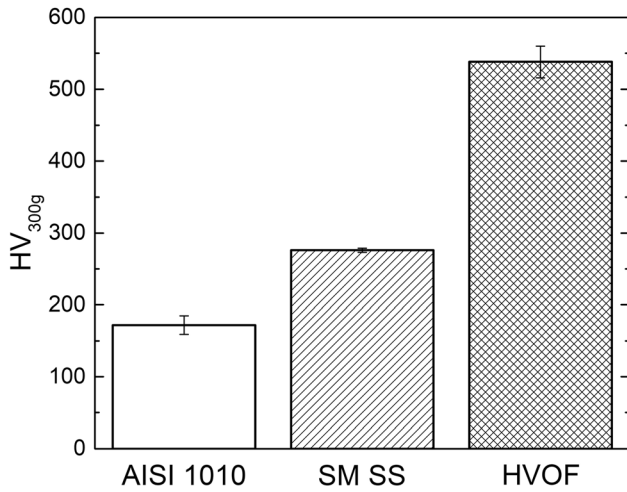


Fig. 7 Vickers hardness, measured at a load of 300 g, of boron-modified supermartensitic stainless steel (SM SS) HVOF coating. Values of the AISI 1010 steel and SM SS included as terms of comparison

of the collected debris, Fig. 11(a), are similar for all testing velocities, and they are similar to the pattern of the original supermartensitic stainless steel. This points out to a similar adhesive wear mechanism regardless of the sliding velocity, but with the severity of material removal increasing for higher velocities. Similar trends are seen for the adhesive wear of the AISI 1010 steel (Fig. 10d-f, 11b), i.e., scars indicating severe plastic deformation and surface damage that increase with the sliding velocity and XRD patterns of the debris similar to the original alloy. The resulting debris can be either the material removed from the disk that remained with the same ferritic structure and/or martensite formed upon deformation. Given the low-carbon content of the AISI 1010 steel, little, if any, lattice distortion in the martensite structure is expected; therefore, a clear distinction of the XRD patterns related to ferrite or martensite is compromised (see Fig. 11b). Whether related to ferrite or martensite, because of the low-carbon content, even if

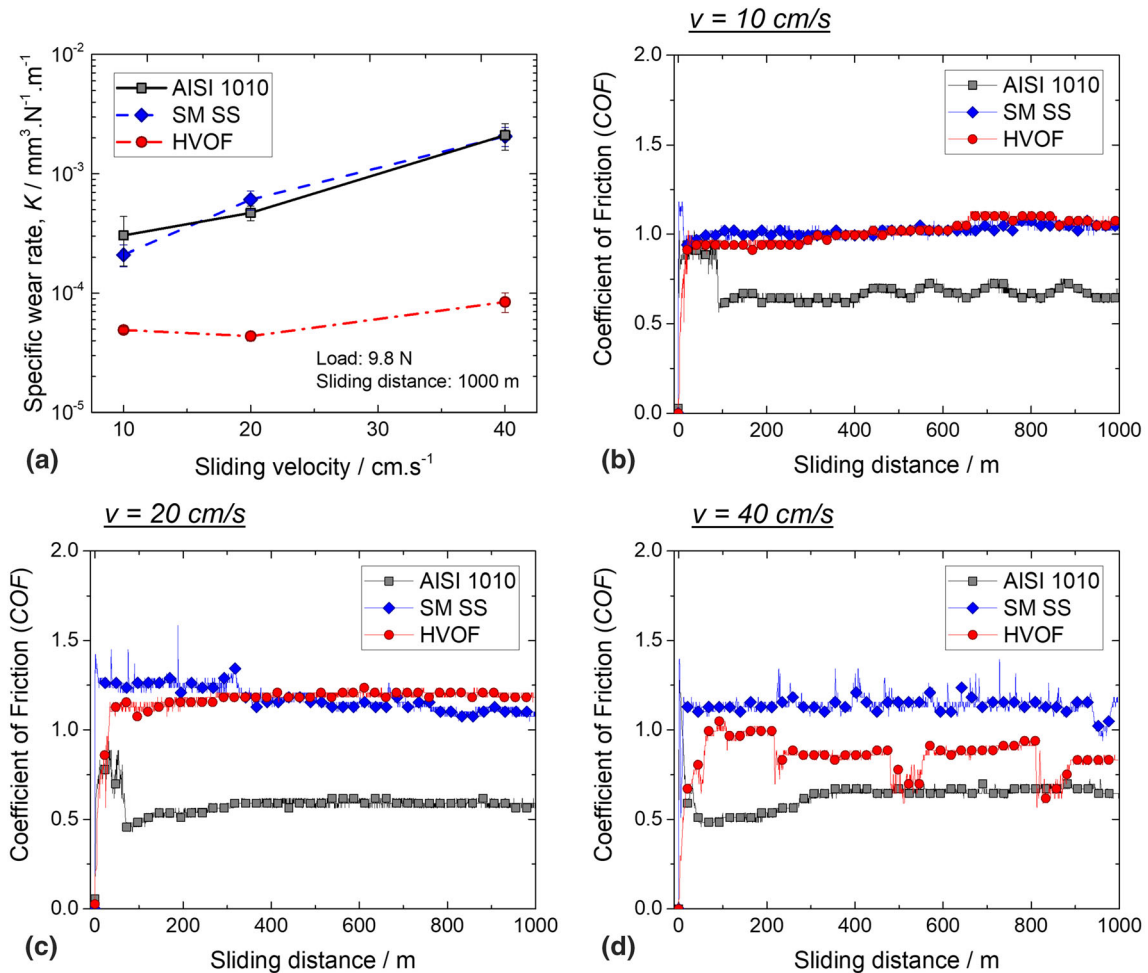
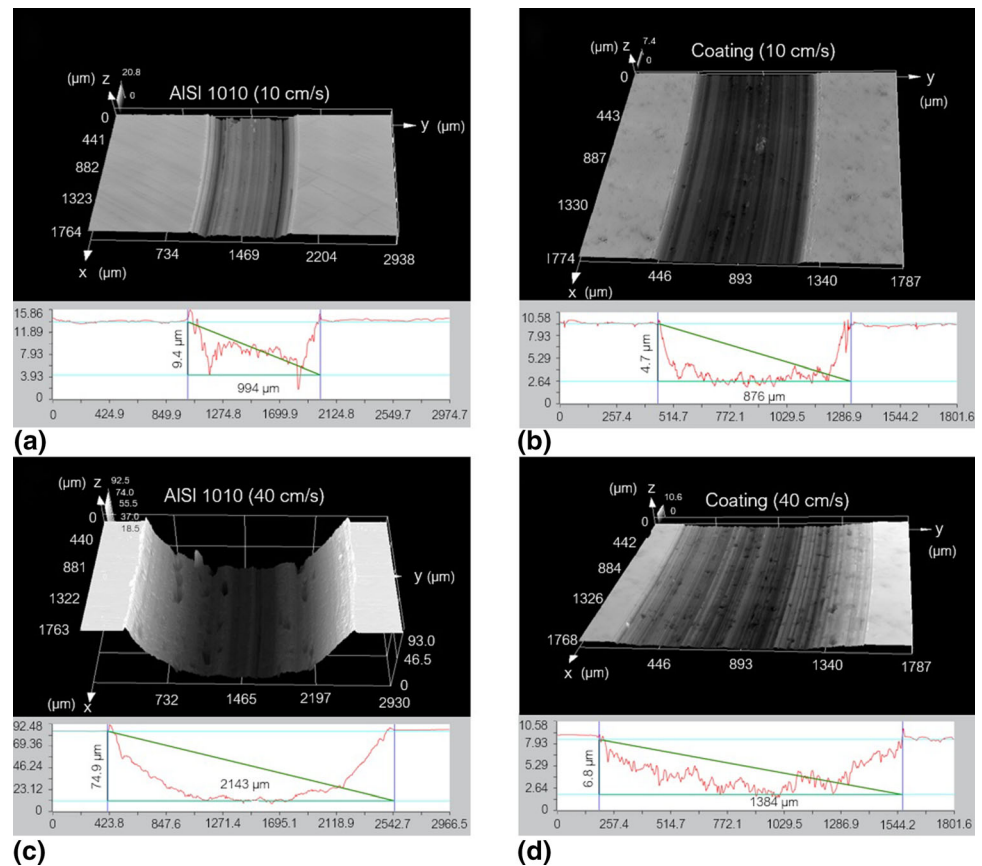


Fig. 8 Specific wear rates (a) and coefficient of friction, *COF*, from pin-on-disk testing of HVOF coatings at different linear velocities: 10 cm/s (b), 20 cm/s (c) and 40 cm/s (d). Results for AISI 1010 steel substrate and supermartensitic stainless steel, SM SS, included for comparison

Fig. 9 Confocal micrographs of the AISI 1010 substrate after testing at (a) 10 cm/s and (b) 40 cm/s, and of the HVOF coating tested at (c) 10 cm/s and (d) 40 cm/s. Indication of the depth and width of the worn surfaces is included



martensite debris is formed, it is not hard and brittle to introduce an abrasive component to the tribosystem. The wear mechanism of the AISI 1010 steel substrate thus remains unchanged, i.e., adhesive wear occurred for all tested conditions.

HVOF coatings, in turn, displayed a different wear mechanism. Worn surfaces after testing at 10 and 20 cm/s, Fig. 10(g) and (h), are smooth but reveal some sites where delamination occurred, typical of coatings with high hardness. The XRD patterns in Fig. 11(c) show peaks related to martensite and oxides. Martensite debris is probably delaminated material from the coating while oxides are some debris particles that oxidized upon wear between the alumina pin and the coating. Delamination theory of wear was introduced by Suh (Ref 33), and it was proved to describe the wear mechanism of some metallic coatings (Ref 34, 35). Indeed, several thermal sprayed coatings display delamination occurrence when submitted to wear (Ref 36–39), generally triggered around the inter-lamellar region. The HVOF coating contains some amount of oxides between the individual particles, as seen in Fig. 6. Oxides are expected to be seen in HVOF coatings when oxidizing flame is employed. Compared to the feedstock powder that contained 0.09% oxygen, the HVOF coating presented 0.93% oxygen. These results suggest the

occurrence of delamination wear for the HVOF coating at sliding velocities of 10 cm/s and 20 cm/s. Figure 12 shows evidence of delamination after testing the HVOF coating at a linear velocity of 20 cm/s. A slightly discontinuous interface gap along the intersplat zone, Fig. 12(a) and (b), is ascribed to the onset of the detachment of material upon wear, Fig. 12(c) and (d), eventually leaving depressions along the surface, Fig. 12(e) and (f).

Grooves are seen in the worn surface in Fig. 10(i), and in more detail in Fig. 13(a), indication of an abrasive fashion during wear at high sliding velocity of 40 cm/s. Indeed, the *COF* fluctuations observed during the wear test of the HVOF coating at 40 cm/s also corroborate with a changing of the wear mechanism. The XRD results in Fig. 11(c) show that for these test conditions the debris is mainly composed of martensite phase (oxide peaks could not be clearly observed) that came from the abrasion of the HVOF coating, suggesting a more severe wear mechanism. Since the composition of the boron-modified super-martensitic stainless steel is poor in carbon (see Table 2), the martensite debris is relatively soft. A more reasonable explanation for the abrasive wear component is the fast incorporation of boride debris into the tribosystem, Fig. 13(b). At the highest sliding velocity (40 cm/s), probably there is a fast removal of soft martensite inside

Fig. 10 Worn surfaces, SEM secondary electrons, of supermartensitic stainless steel master alloy (a, b, c), AISI 1010 steel substrate (d, e, f) and HVOF coatings (g, h, i)

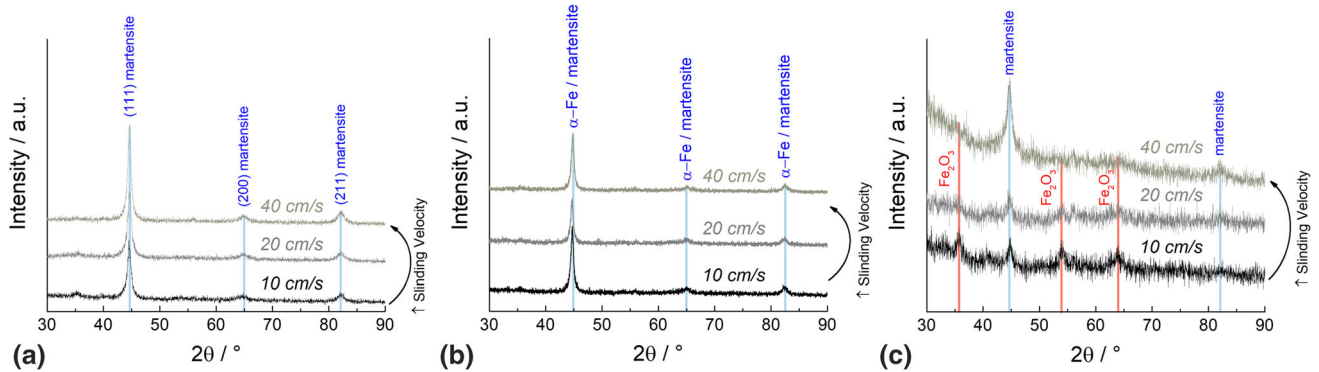
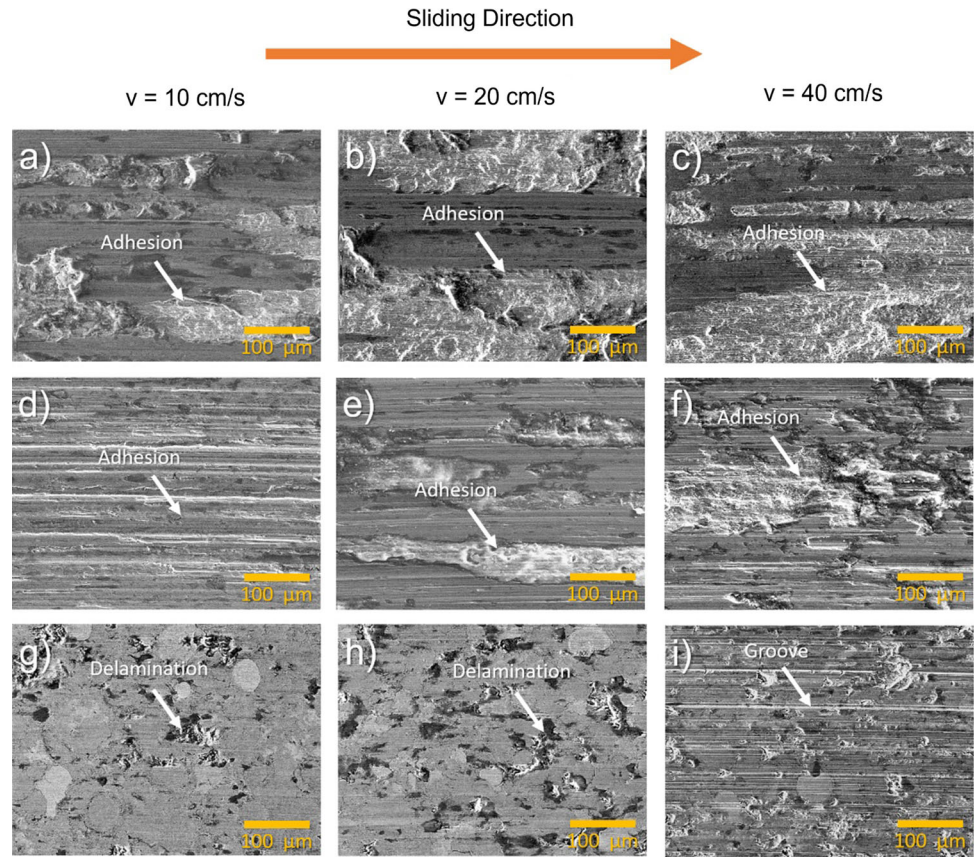


Fig. 11 XRD patterns of the debris of supermartensitic stainless steel master alloy (a), AISI 1010 steel substrate (b) and HVOF coatings (c)

the grains, exposing large fraction of the boride skeleton at the grain boundaries. Being hard but fragile, the borides are eventually fractured, releasing hard debris into the tri-system acting as abrasives. Although associated to higher wear, compared to the other samples tested at 40 cm/s, the HVOF coating still exhibited considerably low specific wear rate values.

From the ensemble of the results and related discussion, boron-modified supermartensitic stainless steel HVOF coatings are interesting wear-resistant solutions to extend the lifespan of inexpensive steel components operating

against hard counterparts. Moreover, owning the processing route, repairing of engineering steels with complex geometries can be performed. Indeed, it was shown that is possible to produce highly wear-resistant coatings that were thick (~ 1000 μm), i.e., suggesting the possibility to reduce the repairing intervals and, therefore, the reduction in the maintenance cost of structural components.

Fig. 12 SEM micrographs after wear testing of the HVOF coating at sliding velocity of 20 cm/s. Different stages of the delamination revealed: (a, b) slight detachment along the intersplat zone, (c, d) increase in the detachment and (e, f) material removal. SE and BSE stand for secondary and backscattered electron micrographs, respectively. Arrows indicate the intersplat zone

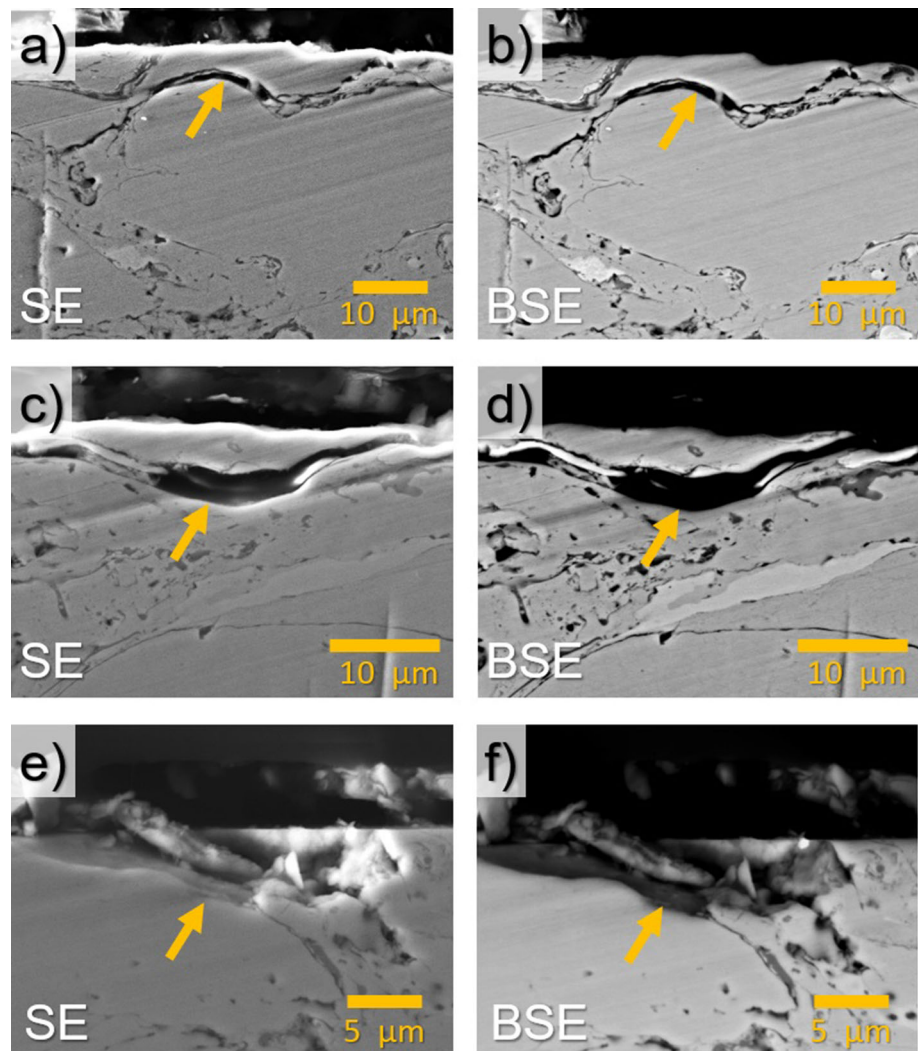
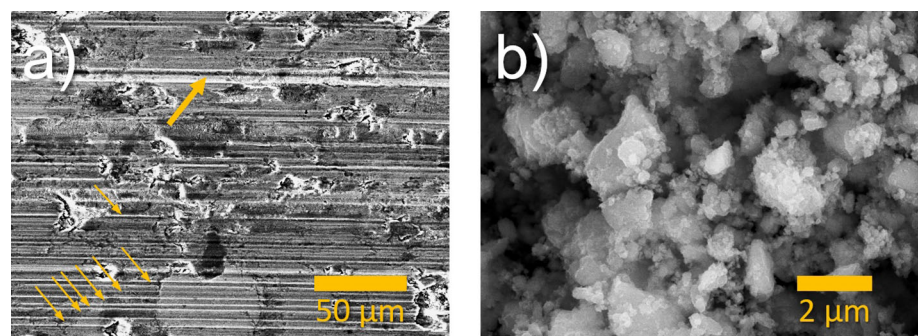


Fig. 13 (a) Worn surface of the HVOF coating after testing at 40 cm/s and (b) resulting debris. SEM micrographs using secondary electron signals. Arrows in (a) indicate grooves due to the abrasive debris incorporation into the tribosystem



Conclusions

- Addition of boron to a commercial supermartensitic stainless steel induces the formation of an interconnected boride network delimiting the grain boundaries. The HVOF process yields to a refined microstructure due to the high cooling rates experienced by the molten particles upon deposition.
- HVOF coatings exhibited higher hardness and lower specific wear rate values when compared to the commercial supermartensitic stainless steel used as master alloy and the AISI 1010 mild steel substrate.
- The commercial supermartensitic stainless steel master alloy and the AISI 1010 mild steel substrate displayed adhesive wear mechanism regardless of the sliding speed. The HVOF coating, in turn, presented

delamination wear at 10 cm/s and 20 cm/s and abrasive wear at 40 cm/s.

- Boron-modified supermartensitic HVOF stainless steels may be used as protective measure to extend the service life of ordinary steel components subjected to wear. Also, these HVOF coatings are interesting for repair of steel structures with complex geometries.

Acknowledgments G. Y. Koga gratefully acknowledges the financial support of FAPESP (post-doctorate fellowship, Grant Number 2017/09237-4). L. S. Silva is thankful for the CNPq funding during his master formation. All authors thank the “Coordenação de Aperfeiçoamento de Pessoal de Nível Superior—Brasil (CAPES)—Finance Code 001” for the financial support. This work was supported by FAPESP (thematic project, Grant Number 2013/05987-8), and by Petrobras S.A. The Villares Metals S.A. is acknowledged for supplying the stainless steels. The authors thank the Laboratory of Structural Characterization (LCE/DEMA/UFSCar) for the general facilities.

Conflict of interest The authors declare that they have no conflict of interest.

References

1. A. Bahadori, *Corrosion and Materials Selection: A Guide for the Chemical and Petroleum Industries*, Wiley, New York, 2014
2. L.N. Moskowitz, Application of HVOF Thermal Spraying to Solve Corrosion Problems in the Petroleum Industry—An Industrial Note, *J. Therm. Spray Technol.*, 1993, **2**(1), p 21–29. <https://doi.org/10.1007/BF02647419>
3. H. Bhadeshia and R. Honeycombe, *Steels: Microstructure and Properties*, 3rd ed., Elsevier, Butterworth-Heinemann, Amsterdam, 2006
4. R.T. Loto, Study of the Corrosion Behaviour of S32101 Duplex and 410 Martensitic Stainless Steel for Application in Oil Refinery Distillation Systems, *J. Mater. Res. Technol.*, 2017, **6**(3), p 203–212. <https://doi.org/10.1016/j.jmrt.2016.11.001>
5. E. McCafferty, *Introduction to Corrosion Science*, 1st ed., Alexandria, Springer-Verlag, New York, 2010. <https://doi.org/10.1007/978-1-4419-0455-3>
6. M. Kulka, Trends in Physical Techniques of Boriding, *Current Trends in Boriding*, 1st ed., M. Kulka, Ed., Gewerbestrasse, Springer Nature, Switzerland, 2019, p 99–253. https://doi.org/10.1007/978-3-030-06782-3_5
7. T.P. Lopes, J. Soyama, G. Zepon, A.R.C. Nascimento, A. Costa e Silva, C.S. Kiminami, W.J. Botta, and C. Bolfarini, Thermodynamic Calculations for the Investigation of Phase Formation in Boron-Modified Ferritic Stainless Steel, *J. Phase Equilibria Diffus.*, 2017, **38**(3), p 343–349. <https://doi.org/10.1007/s11669-017-0550-y>
8. G.Y. Koga, R.P. Nogueira, V. Roche, A.R. Yavari, A.K. Melle, J. Gallego, C. Bolfarini, C.S. Kiminami, and W.J. Botta, Corrosion Properties of Fe-Cr-Nb-B Amorphous Alloys and Coatings, *Surf. Coatings Technol.*, 2014, **254**, p 238–243. <https://doi.org/10.1016/j.surfcoat.2014.06.022>
9. G. Zepon, C.S. Kiminami, W.J. Botta Filho, and C. Bolfarini, Microstructure and Wear Resistance of Spray-Formed Supermartensitic Stainless Steel, *Mater. Res.*, 2013, **16**(3), p 642–646. <https://doi.org/10.1590/s1516-14392013005000026>
10. G. Zepon, A.R.C. Nascimento, A.H. Kasama, R.P. Nogueira, C.S. Kiminami, W.J. Botta, and C. Bolfarini, Design of Wear Resistant Boron-Modified Supermartensitic Stainless Steel by Spray Forming Process, *Mater. Des.*, 2015, **83**, p 214–223. <https://doi.org/10.1016/j.matdes.2015.06.020>
11. J. Soyama, G. Zepon, T.P. Lopes, L. Beraldo, C.S. Kiminami, W.J. Botta, and C. Bolfarini, Microstructure Formation and Abrasive Wear Resistance of a Boron-Modified Superduplex Stainless Steel Produced by Spray Forming, *J. Mater. Res.*, 2016, **31**(19), p 2987–2993. <https://doi.org/10.1557/jmr.2016.323>
12. J. Soyama, T.P. Lopes, G. Zepon, C.S. Kiminami, W.J. Botta, and C. Bolfarini, Wear Resistant Duplex Stainless Steels Produced by Spray Forming, *Met. Mater. Int.*, 2019, **25**(2), p 456–464. <https://doi.org/10.1007/s12540-018-0202-8>
13. G. Koga, L. Otani, A. Silva, V. Roche, R. Nogueira, A. Jorge, C. Bolfarini, C. Kiminami, and W. Botta, Characterization and Corrosion Resistance of Boron-Containing-Austenitic Stainless Steels Produced by Rapid Solidification Techniques, *Materials (Basel)*, 2018, **11**(11), p 2189. <https://doi.org/10.3390/ma11112189>
14. E.V. Shadrachev and A.E. Ivanov, Relative Wear-Resistance of Single-Phase and Two-Phase Boride Layers, *Met. Sci. Heat Treat.*, 1984, **26**(3), p 235–239. <https://doi.org/10.1007/BF00703870>
15. P.S. Grant, Solidification in Spray Forming, *Metall. Mater. Trans. A*, 2007, **38**(7), p 1520–1529. <https://doi.org/10.1007/s11661-006-9015-3>
16. P.S. Grant, Spray Forming, *Prog. Mater. Sci.*, 1995, **39**(4–5), p 497–545. [https://doi.org/10.1016/0079-6425\(95\)00004-6](https://doi.org/10.1016/0079-6425(95)00004-6)
17. J.R. Davis, *Surface Engineering for Corrosion and Wear*, ASM International, Materials Park, 2001
18. L. Pawlowski, *The Science and Engineering of Thermal Spray Coatings*, 2nd ed., Wiley, New York, 2008. <https://doi.org/10.1002/9780470754085>
19. M. Li and P.D. Christofides, Modeling and Control of High-Velocity Oxygen-Fuel (HVOF) Thermal Spray: A Tutorial Review, *J. Therm. Spray Technol.*, 2009, **18**(5–6), p 753–768. <https://doi.org/10.1007/s11666-009-9309-2>
20. J.R. Davis, Introduction to Thermal Spray Processing, *Handbook of Thermal Spray Technology*, 1st ed., J.R. Davis, Ed., ASM International, Materials Park, 2004, p 3–13
21. T.C. Totemeier, Effect of High-Velocity Oxygen-Fuel Thermal Spraying on the Physical and Mechanical Properties of Type 316 Stainless Steel, *J. Therm. Spray Technol.*, 2005, **14**(3), p 369–372. <https://doi.org/10.1361/105996305X59440>
22. Z. Zhou, L. Wang, D.Y. He, F.C. Wang, and Y.B. Liu, Microstructure and Wear Resistance of Fe-Based Amorphous Metallic Coatings Prepared by HVOF Thermal Spraying, *J. Therm. Spray Technol.*, 2010, **19**(6), p 1287–1293. <https://doi.org/10.1007/s11666-010-9556-2>
23. S.A. Galedari, A. Mahdavi, F. Azarmi, Y. Huang, and A. McDonald, A Comprehensive Review of Corrosion Resistance of Thermally-Sprayed and Thermally-Diffused Protective Coatings on Steel Structures, *J. Therm. Spray Technol.*, 2019, **28**(4), p 645–677. <https://doi.org/10.1007/s11666-019-00855-3>
24. B.S. Yilbas, M. Khalid, and B.J. Abdul-Aleem, Corrosion Behavior of HVOF Coated Sheets, *J. Therm. Spray Technol.*, 2003, **12**(4), p 572–575. <https://doi.org/10.1361/105996303772082323>
25. H.-J. Kim, S. Grossi, and Y.-G. Kweon, Characterization of Fe-Cr-B Based Coatings Produced by HVOF and PTA Processes, *Met. Mater.*, 1999, **5**(1), p 63–72. <https://doi.org/10.1007/BF03026006>
26. H.-J. Kim, S. Grossi, and Y.-G. Kweon, Wear Performance of Metamorphic Alloy Coatings, *Wear*, 1999, **232**(1), p 51–60. [https://doi.org/10.1016/S0043-1648\(99\)00160-X](https://doi.org/10.1016/S0043-1648(99)00160-X)

27. H.-J. Kim, B.-H. Yoon, and C.-H. Lee, Wear Performance of the Fe-Based Alloy Coatings Produced by Plasma Transferred Arc Weld-Surfacing Process, *Wear*, 2001, **249**(10-11), p 846-852. [https://doi.org/10.1016/S0043-1648\(01\)00683-4](https://doi.org/10.1016/S0043-1648(01)00683-4)
28. G.Y. Koga, R. Schulz, S. Savoie, A.R.C. Nascimento, Y. Drolet, C. Bolfarini, C.S. Kiminami, and W.J. Botta, Microstructure and Wear Behavior of Fe-Based Amorphous HVOF Coatings Produced from Commercial Precursors, *Surf. Coatings Technol.*, 2017, **309**, p 938-944. <https://doi.org/10.1016/j.surfcoat.2016.10.057>
29. G.Y. Koga, W. Wolf, R. Schulz, S. Savoie, C. Bolfarini, C.S. Kiminami, and W.J. Botta, Corrosion and Wear Properties of FeCrMnCoSi HVOF Coatings, *Surf. Coatings Technol.*, 2019, **357**, p 993-1003. <https://doi.org/10.1016/j.surfcoat.2018.10.101>
30. G.Y. Koga, A.M. Jorge Junior, V. Roche, R.P. Nogueira, R. Schulz, S. Savoie, A.K. Melle, C. Loable, C. Bolfarini, C.S. Kiminami, and W.J. Botta, Production and Corrosion Resistance of Thermally Sprayed Fe-Based Amorphous Coatings from Mechanically Milled Feedstock Powders, *Metall. Mater. Trans. A*, 2018, **49**(10), p 4860-4870. <https://doi.org/10.1007/s11661-018-4785-y>
31. I. Hutchings and P. Shipway, *Tribology: Friction and Wear of Engineering Materials: Second Edition*, 2nd ed., Butterworth-Heinemann, Oxford, 2017
32. J.R. Davis, D.E. Crawmer, and Thermal Spray Technologies Inc., Coating Structures, Properties, and Materials, *Handbook of Thermal Spray Technology*, 1st ed., J.R. Davis, Ed., ASM International, Materials Park, 2004, p 47-53
33. N.P. Suh, The Delamination Theory of Wear, *Wear*, 1973, **25**(1), p 111-124. [https://doi.org/10.1016/0043-1648\(73\)90125-7](https://doi.org/10.1016/0043-1648(73)90125-7)
34. S. Jahanmir, N.P. Suh, and E.P. Abrahamson, The Delamination Theory of Wear and the Wear of a Composite Surface, *Wear*, 1975, **32**(1), p 33-49. [https://doi.org/10.1016/0043-1648\(75\)90203-3](https://doi.org/10.1016/0043-1648(75)90203-3)
35. S. Jahanmir, E.P. Abrahamson, and N.P. Suh, Sliding Wear Resistance of Metallic Coated Surfaces, *Wear*, 1976, **40**(1), p 75-84. [https://doi.org/10.1016/0043-1648\(76\)90019-3](https://doi.org/10.1016/0043-1648(76)90019-3)
36. B. Xu, Z. Zhu, S. Ma, W. Zhang, and W. Liu, Sliding Wear Behavior of Fe-Al and Fe-Al/WC Coatings Prepared by High Velocity Arc Spraying, *Wear*, 2004, **257**(11), p 1089-1095. <https://doi.org/10.1016/j.wear.2004.05.012>
37. B. Huang, C. Zhang, G. Zhang, and H. Liao, Wear and Corrosion Resistant Performance of Thermal-Sprayed Fe-Based Amorphous Coatings: A Review, *Surf. Coatings Technol.*, 2019, **377**(4), p 124896. <https://doi.org/10.1016/j.surfcoat.2019.124896>
38. Q. Luo, Y.J. Sun, J. Jiao, Y.X. Wu, S.J. Qu, and J. Shen, Formation and Tribological Behavior of AC-HVAF-Sprayed Non-ferromagnetic Fe-Based Amorphous Coatings, *Surf. Coatings Technol.*, 2018, **334**, p 253-260. <https://doi.org/10.1016/j.surfcoat.2017.11.042>
39. G. Bolelli, A. Milanti, L. Lusvardi, L. Trombi, H. Koivuluoto, and P. Vuoristo, Wear and Impact Behaviour of High Velocity Air-Fuel Sprayed Fe-Cr-Ni-B-C Alloy Coatings, *Tribol. Int.*, 2016, **95**, p 372-390. <https://doi.org/10.1016/j.triboint.2015.11.036>

Publisher's Note Springer Nature remains neutral with regard to jurisdictional claims in published maps and institutional affiliations.